Consequences of the balance between the repulsive and attractive forces in dense, nonassociated liquids

Randall A. LaViolette and Frank H. Stillinger
AT&T Bell Laboratories, Murray Hill, New Jersey 07974

(Received 3 December 1984; accepted 14 December 1984)

Current theories successfully predict the equilibrium structure of many simple liquids near their triple point from the repulsive molecular forces alone. We present a simple model substance whose liquid structure cannot be predicted adequately with only the repulsions. Furthermore, the model's crystal structure changes drastically upon the removal of the attractions. This failure for our model to conform to the accepted picture of simple liquids gives us the opportunity to sharpen the boundary between substances which, respectively, may and may not be expected to so conform. We conclude that the structure of the corresponding solid deserves more weight than is conventionally given by modern theories of liquids.

I. INTRODUCTION

One of the central goals of liquid state theory is an understanding of the structure of liquids in terms of the forces between the interacting molecules. The most successful theoretical descriptions of dense, one-component, nonassociated liquids have the van der Waals picture as their basic physical ingredient.[1-3] In the van der Waals picture, the repulsive forces alone determine the structure of the liquid, while the attractive forces may be either neglected altogether, or incorporated into only the lowest order of corrections.

The justification of the van der Waals picture usually begins by considering the force between an isolated pair of the atoms or molecules which constitute a dense, nonassociated, one-component liquid.[1,2] For example, a glance at the radial force given by the Lennard-Jones model, illustrated in Fig. 1(b), shows that the repulsive force from the nearest neighbors is much stronger and more rapidly varying than the attractive force from all the neighbors. At the high densities typical of a liquid at or above its triple-point temperature, the average distance between the nearest neighbors is small enough for the repulsive force to dominate almost completely the attractive force. Although these conclusions are strictly correct only in the limit of high density and temperature, in practice, theories based upon the van der Waals picture have successfully predicted the structure of many atomic and molecular liquids even at their triple point.[1] The same may be said of many solids as well, and in such cases, the van der Waals picture provides the basis for simple, successful theories of the liquid–solid phase transition.[4]

Those who have advanced the van der Waals picture for such liquids have also outlined some exceptions.[1,5] For example, near the critical point, the density is too low and the compressibility is too high to regard the liquid simply as a collection of repulsive particles. The van der Waals picture is also inadequate whenever the attractive forces are so strong, directional, and rapidly varying that they can be clearly seen to counterbalance the repulsive forces in an important way. Associated liquids such as water and the alcohols are examples of substances where such a balance is clearly visible. Mixtures of two or more species, charged or not, can provide another example of a liquid where attractive forces can balance or offset repulsive forces. Even so, there is a wide variety of atomic and molecular liquids which substantially conform to the van der Waals picture. A reader of the review literature[1-3] is entitled to expect that a simple physical atomic liquid is adequately described by the van der Waals picture at densities and temperatures at or not too far above the triple point.

The boundary between substances which would, and would not, be expected to conform to the van der Waals picture is at the moment, however, hazy. We propose to sharpen the vision of that boundary with the study of a model simple atomic liquid which we call "hexon," (so-called both for the similarity of its potential to those which model noble gases, and for the hexagonal symmetry of its crystal, which we discuss in succeeding sections.) In the next section we will compare the hexon model to the venerable and thoroughly studied[1-3] Lennard-Jones model, since the latter yields both an atomic liquid and solid which conform to the van der Waals picture.[4] With this comparison, we intend to show that, according to conventional expectations, the hexon pair potential should yield a liquid which also conforms to the van der Waals picture. In the succeeding sections we will discuss the results of molecular dynamics calculations for liquid and solid hexon near its triple point. We will see that the structure of both the solid and liquid hexon diverge from the van der Waals picture, despite orthodox expectations.

II. HEXON vs LENNARD-JONES

The hexon pair potential $u(r)$ belongs to the class of potentials described below[6]:

$$u(r) = A \exp[(r-a)^{-1}](r^{-p} - r^{-q}), \quad r < a,$$
$$= 0, \quad r \geq a.$$

 0021-9606/85/073335-09$02.10

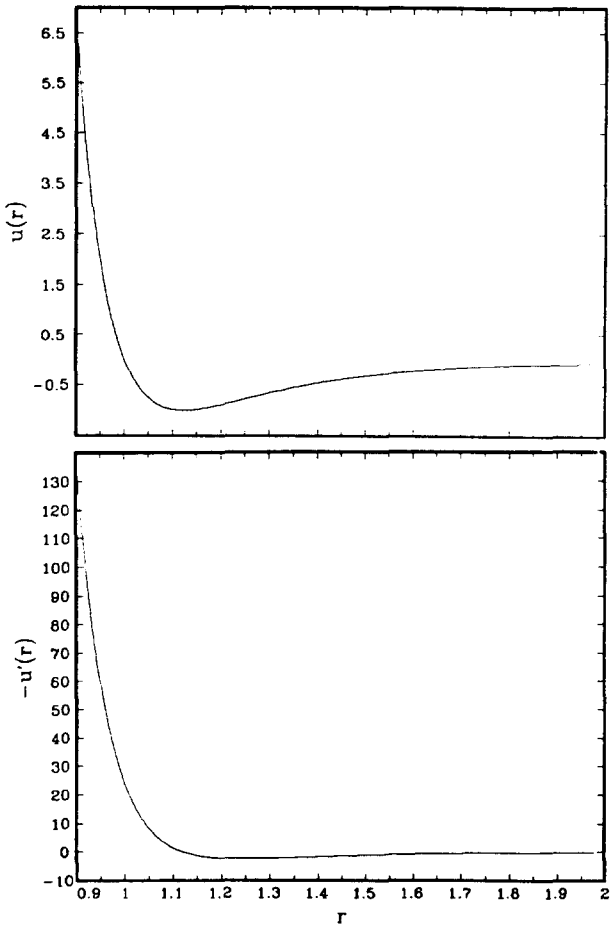

FIG. 1. (a) The pair potential for the Lennard-Jones model is shown in the upper panel and (b) the radial force $-u'(r)$ is shown in the lower panel.

The parameter a fixes the length of the interaction, so that the potential is smoothly cut off at $r = a$. With appropriate choices for the parameters, Stillinger and Weber made $u(r)$ essentially a smoothly cutoff Lennard-Jones pair potential with $\epsilon = \sigma = 1$. For the hexon model we (arbitrarily) chose the parameters $p = 12$, $q = -3$, and $a = 2$. With these choices, the minimum was found at $r_e = 1.348\,076\,907$. We chose $A = 1.914\,166\,098$ so that at the minimum, $u(r_e) = -1$.

The hexon model is similar in several respects to the Lennard-Jones model, for $\epsilon = \sigma = 1$. The pair potentials are illustrated in Figs. 1(a) and 2(a). Like the Lennard-Jones model, the hexon pair potential is radially symmetric, and has only one minimum. Since it is important to the argument for the van der Waals picture, we discuss in detail the repulsive and attractive forces for both of the models. The radial force $-u'(r)$ for each of the two models is illustrated in Figs. 1(b) and 2(b). The radial force is repulsive where it is positive, and attractive where negative.

In both models, the repulsive part is much stronger and more rapidly varying than the attractive part of the force. At $r = 0.9$, (inside roughly 1/10 the diameter of either the hexon or the Lennard-Jones atom), the repulsive force for *either* model is at least an order of magnitude stronger than the attractive force is at any distance. The range of the repulsive force for the hexon is in one respect longer than that for the Lennard-Jones model, since the minimum of the hexon potential r_e is farther from the origin than is r_e for the Lennard-Jones model. The repulsive force for the hexon model is not nearly so strong or rapidly varying as it is for the Lennard-Jones model. At $r = 0.9$ it is about one-third as strong as for the Lennard-Jones model. However, we emphasize that we are not testing whether or not a *hard-sphere* model would adequately reproduce the liquid structure.[7] We neither expect nor insist that a theory which describes the repulsions in terms of hard-sphere repulsions would successfully calculate the structure of the dense liquid hexon. If we accept the van der Waals picture, we should only require that the true repulsive forces, not necessarily hard-sphere repulsive forces, will themselves correctly reproduce the structure of the dense liquid, as long as they are much stronger than the attractive forces.

As far as the van der Waals picture is concerned, the only issue remaining is whether or not the attractive force can effectively counterbalance the repulsive force. We show only a part of the radial force for both models in Fig. 3. We do this because, in Figs. 1(b) and 2(b), the contrast between the attractive and the repulsive force, in both models, is so great, that the difference between the

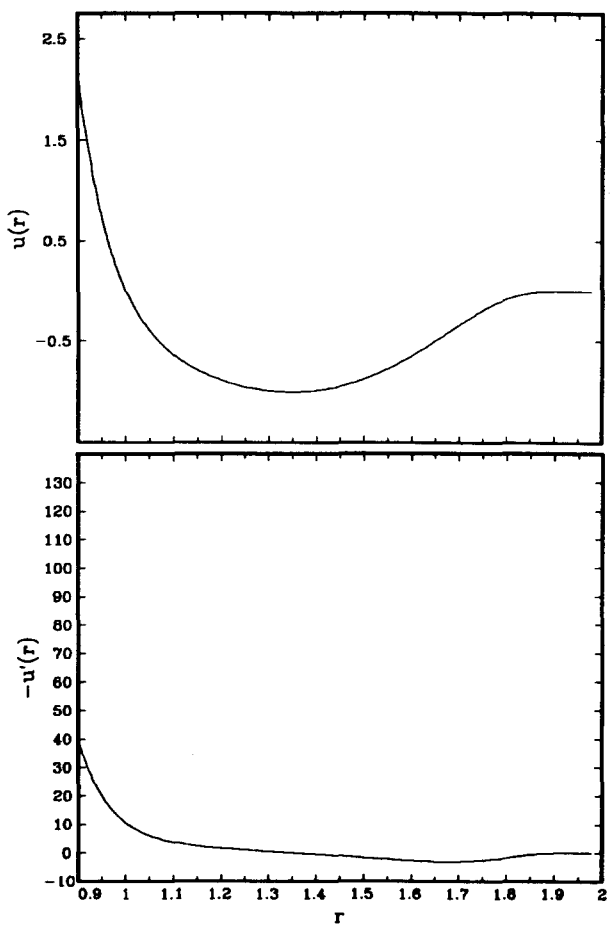

FIG. 2. (a) The pair potential for the hexon model is shown in the upper panel and (b) the radial force $-u'(r)$ is shown in the lower panel.

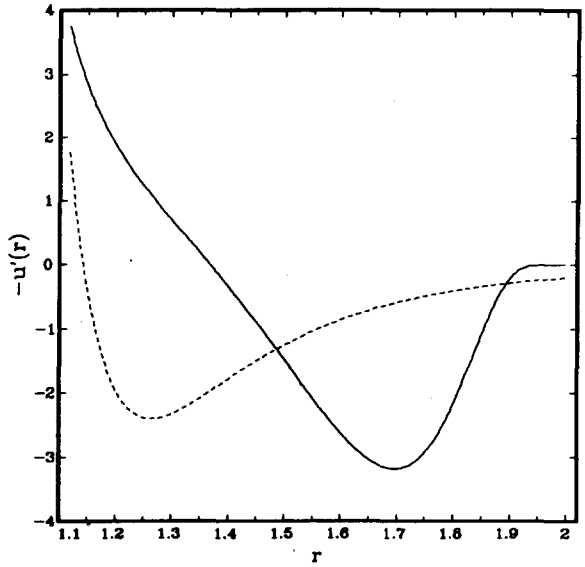

FIG. 3. Detail of Figs. 1(b) and 2(b). The radial force for the hexon model is drawn with the solid curve, and that for the Lennard-Jones model is drawn with the dashed curve.

two attractive forces is difficult to see. According to conventional expectations, this is itself a pictorial indication that the hexon, as well as the Lennard-Jones liquid, should conform to the van der Waals picture. In Fig. 3, it is easier to see that the attractive force for the hexon model is scarcely stronger or more rapidly varying than it is for the Lennard-Jones model. Perhaps the most obvious difference between them is that the attractive force for the hexon model is strongest at $r = 1.68$, while for the Lennard-Jones model it is strongest at $r = 1.24$. Yet these differences in shape should not be important if the van der Waals picture is appropriate, since the attractive forces in both models are radially symmetric and vary only about 2ϵ per unit distance over the range of attractions.[8] This comparison of only the attractive force for the hexon model with that in the Lennard-Jones model gives us no reason to suppose that attractive force could counterbalance the repulsive force in any significant way, for either model.

We would thus expect that the van der Waals picture should provide a reasonably accurate description of the liquid hexon, and perhaps of the solid hexon as well. In the following sections we test this expectation with the results of molecular dynamics calculations for the structure of the liquid and solid hexon near its triple point.

III. A CRITERION FOR CONFORMITY TO THE VAN DER WAALS PICTURE

In the strict van der Waals picture, repulsive forces alone determine the structure of a dense solid or liquid. The structure of an atomic solid or liquid is usually represented[9] by the radial distribution function $g(r)$. The van der Waals picture therefore may be presented[1,2,4] as the assertion that $g(r) = g_0(r)$, for all temperatures, where $g_0(r)$ is the radial distribution function determined solely by the repulsive forces between the atoms. This equality will not be exactly obeyed for physically reasonable model interactions.[10] Weeks and Broughton[4] have discussed in detail the difference between $g(r)$ and $g_0(r)$ for both the Lennard-Jones liquid and solid near the triple point. Although the differences are in each case perceptible, for our purposes they are negligible. In the present context, we will agree that a solid or liquid indeed conforms to the van der Waals picture if, for that solid or liquid near the triple point, the equality $g(r) = g_0(r)$ is maintained as well as it is for the Lennard-Jones solid or liquid at comparable temperature and density. Of course, we expect that any classical liquid at sufficiently high temperatures and densities will conform in a trivial fashion to the van der Waals picture. We are only concerned with the more interesting regime of temperatures and densities near the triple point of that substance.

In order to calculate $g_0(r)$, the pair potential $u(r)$ should be separated into the sum of two terms: the "core" potential $u_0(r)$, corresponding to the repulsive force, and the remainder $v(r)$, corresponding to the attractive force. Following Weeks, Chandler, and Andersen,[1,2] we write the core potential for hexon as

$$u_0(r) = u(r) - u(r_e), \quad r \le r_e,$$
$$= 0, \quad r > r_e.$$

We will always use the subscript "0" to refer only to properties of the core potential.

In the following sections we will compare $g(r)$ for the hexon solid and liquid, to the $g_0(r)$ for the core solid and liquid, as calculated by molecular dynamics.

IV. THE STRUCTURE OF THE SOLID HEXON COMPARED TO THE VAN DER WAALS PREDICTION

Our comparison of the structure of the core solid with the hexon solid near the triple point of hexon begins with a discussion of the crystal structure of each model at zero temperature and pressure. The density which yields the zero pressure structure of hexon at zero temperature is near the triple-point density, and the temperature for which the hexon solid melts is near the triple-point temperature. We then compare $g(r)$ for the hexon solid with $g_0(r)$ for the core solid, calculated at a density and temperature below the hexon triple point.

A. The structure of the hexon crystal at $T = 0$ and $P = 0$

We have examined all monatomic Bravais lattices, the diamond lattice, and the hexagonal close-packed lattice[11] in order to identify the structure with the lowest potential energy at zero temperature and pressure. For the diamond and hexagonal close-packed lattices, we simply calculated and compared the lattice energy,

$$U = \sum_{\mathbf{r}} u(|\mathbf{r}|), \quad \mathbf{r} \in \{\text{lattice}\}$$

over a wide range of densities $\rho = 1/v$, where v is the volume of the unit cell. In order to search among all

monatomic Bravais lattices, we combined a steepest-descent and a conjugate-gradient procedure[12] to minimize U with respect to the length and orientation of each of the basis vectors, for a fixed volume v of the unit cell. The conjugate-gradient technique guarantees that the calculated force constants are positive, so that the structure indeed represents a local minimum rather than a maximum or a saddle point on the potential energy surface. No boundary conditions were applied in this search; they were not required with our short-ranged potentials. For densities from 0.78 to 1.35, the only Bravais lattices for which U was a minimum were simple hexagonal lattices. For lower densities, only simple cubic lattices were found. For many densities in this range, we repeated the minimization from several different and randomly selected configurations. In every case the basis vectors were reproducible to at least six significant figures.

In Fig. 4 we show the energies corresponding to the diamond, hexagonal close-packed, simple cubic, and simple hexagonal lattices as a function of density. We will focus on the zero pressure case since we expect that the corresponding density will be near the triple density. At zero pressure, the simple hexagonal lattice is the one which corresponds to the lowest energy for the hexon potential. The energy per particle is $U/N = -7.380\,685\,5$, and the density is $\rho = 0.8895$.

The simple hexagonal lattice can be constructed by stacking layers of two-dimensional triangular nets directly above one another, a distance c apart.[11] Each net, which is itself a two-dimensional close-packed lattice, consists of atoms placed at the vertices of equilateral triangles with sides of length a. The parameters a and c are listed in Table I for a few densities which correspond to low-pressure structures. At these densities, U is lowest for these simple hexagonal structures.

TABLE I. Cell parameters a and c for the simple hexagonal lattice found at $T = 0$ and density ρ for the hexon model. The zero-pressure structure is found at the density $\rho = 0.8895$.

ρ	a	c	c/a
0.800 000	1.178 959	1.038 441	0.880 811
0.820 000	1.166 373	1.035 096	0.887 448
0.850 000	1.148 314	1.030 219	0.897 158
0.880 605	1.130 910	1.025 260	0.906 580
0.889 500	1.126 044	1.023 795	0.909 196
0.898 395	1.121 261	1.022 323	0.911 762
0.900 000	1.120 407	1.022 057	0.912 220
0.950 000	1.094 308	1.015 002	0.927 529
1.050 000	1.037 131	1.022 382	0.985 780
1.150 000	0.999 520	1.005 053	1.005 536
1.250 000	0.973 444	0.974 850	1.001 444

The simple hexagonal lattice is remarkable in several respects. While the hexon model is one of a class of atomic pair-potential models, the simple hexagonal phase has not been found for any of the elements at low pressures.[13] Also, most of the elements which do crystallize into hexagonally symmetric structures do so with a c/a ratio larger than unity and near the "ideal" close-packed ratio of 1.633.[13] However, the hexon crystal has a c/a ratio less than unity for the densities which correspond to low pressures. We show how the c/a ratio varies with density in Table I. When c/a is less than unity, the nearest neighbors of an atom are not the six surrounding atoms in its own (close-packed) layer, but instead are the two atoms in the layers directly above and below it. This feature is vividly displayed in the radial distribution function shown for the zero pressure structure in Fig. 5, for $T = 2 \times 10^{-5}$. For example, what would have been the first and third peaks for a c/a ratio of unity have each

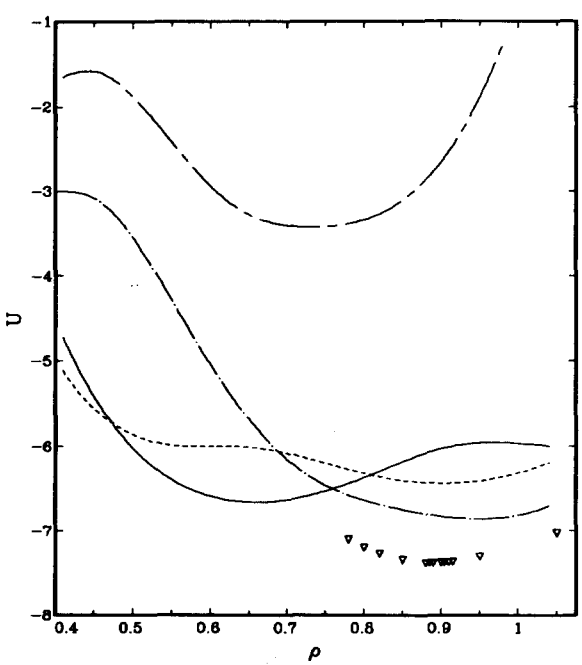

FIG. 4. The potential energy U at $T = 0$, as a function of density ρ, for the following structures: diamond (chain-dash curve), simple cubic (chain-dot curve), hexagonal close packed (dashed curve), body-centered cubic (solid curve), and, the simple hexagonal structures (triangles) found by the conjugate-gradient minimization of U.

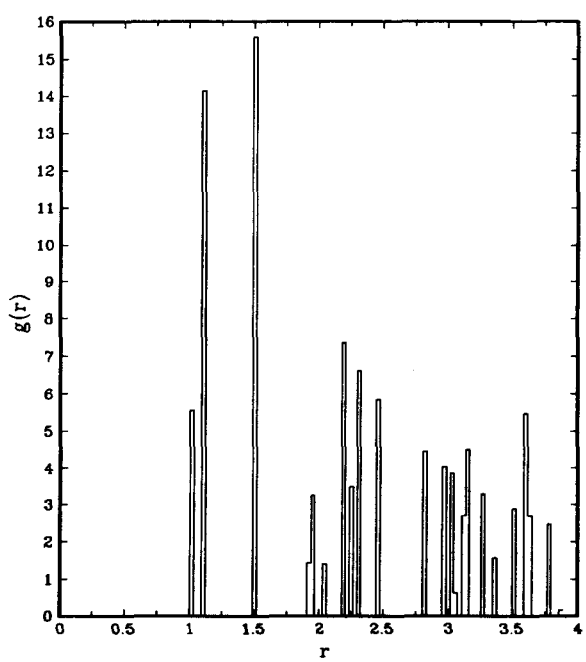

FIG. 5. The radial distribution function for the hexon crystal at $T = 2 \times 10^{-5}$ and $\rho = 0.8895$. The bin is 0.03 wide.

been split into two peaks. For many structures, the maximum of the radial distribution function is in the first peak, but here, it is a maximum in the third peak. Finally, the simple hexagonal lattice is a loosely packed structure in comparison to the face-centered cubic, body-centered cubic, and hexagonal close-packed structures commonly found for the elements. In Table II we show the packing fractions[11] calculated for the zero-pressure hexon crystal structure, and for some of the structures found for the elements. It would be remarkable if a potential with only a repulsive force could produce such a structure. Even potentials with a repulsive force much softer than that for the hexon potential are not known to produce structures more loosely packed than the body-centered cubic lattice.[14] We nevertheless continue with our comparison of the hexon solid with the van der Waals prediction for the solid structure, as we present the crystal structure corresponding to the core potential.

B. The crystal structure for the core potential

We found the zero pressure hexon crystal at the density $\rho = 0.8895$, and so we look for the crystal structure for the core potential by comparing the lattice energy

$$U_0 = \sum_{\mathbf{r}} u_0(|\mathbf{r}|), \quad \mathbf{r} \in \{\text{lattice}\}$$

for a variety of lattices at that density. We calculated U_0 for the body-centered cubic, face-centered cubic, simple cubic, hexagonal close-packed, and diamond lattices for the range of densities shown in Fig. 6. We also calculated U_0 for all simple hexagonal lattices at the density $\rho = 0.8895$. Only the difference between the energies for the body and face-centered cubic lattices is shown in Fig. 6; U_0 for the hexagonal close-packed lattice is virtually identical to U_0 for the face-centered cubic lattice, and the energy for the others is always much higher than either of the two lattices. For densities from 0.8600 to 1.0600, U_0 is lowest for the body-centered cubic lattice.

The fact that the repulsive force of the hexon model produces a crystal structure less closely-packed (cf. Table II) than the structure for the Lennard-Jones crystal indicates that the repulsive force of the hexon model is qualitatively "softer" than the repulsive force of the Lennard-Jones model.[15] The softness of the hexon's repulsive force may be considered unusual but should not be reckoned unphysical. For example, if the van der Waals picture is appropriate for any substance (e.g., alkali metals) with a body-centered cubic crystal,[1] the repulsions will be comparably soft.

TABLE II. The packing fraction of the simple hexagonal lattice at $\rho = 0.8895$ compared with some other lattices (Ref. 11). The packing fraction for any simple hexagonal lattice is found from $\pi \cdot 3^{-3/2} \cdot (c/a)^2$.

Lattice	Packing fraction
face-centered-cubic	0.74
body-centered-cubic	0.68
simple-hexagonal	0.55
simple-cubic	0.52
diamond	0.34

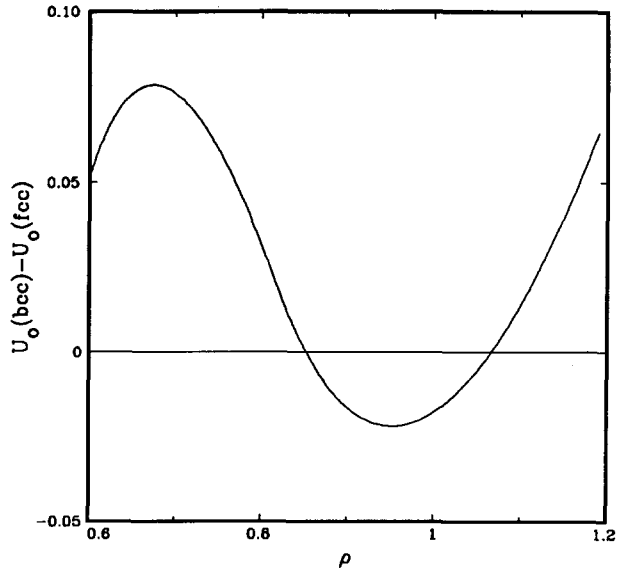

FIG. 6. The difference $U_0^{\text{bcc}} - U_0^{\text{fcc}}$ as a function of density for the core potential at $T = 0$.

If the van der Waals picture were accurate for hexon at zero temperature and pressure, then the crystal structure found from the core potential at the same density ($\rho = 0.8895$) should have been the structure found for hexon. Here, however, the attractive force balances the repulsive force in an important way for hexon. This failure of the van der Waals picture in this circumstance should not be taken, by itself, to be a counterexample to the van der Waals picture. The van der Waals picture assumes high temperatures, and the most that is usually claimed for the van der Waals picture is that it is accurate even down to triple-point temperatures. Therefore, the real test of the van der Waals picture for the solid and the liquid is found when we adjust the temperature, via molecular dynamics, to near the triple-point temperature. After a brief discussion of the molecular dynamics calculation, we will compare the structure of the solid and liquid predicted by the van der Waals picture with the actual structure.

V. DETAILS OF THE MOLECULAR DYNAMICS CALCULATION

Molecular dynamics was executed, respectively, for 448 hexon and 432 core atoms. The volume of each of the boxes was chosen so that the density was $\rho = 0.8895$. The box of the 432 core atoms was constructed as a cube with sides of length $6 \cdot 2^{1/2} \cdot \rho^{-1/3}$ so that it would be commensurate with the body-centered cubic lattice. The box for the 448 hexon atoms was constructed with sides of length $7 \cdot a$, $4 \cdot 3^{1/2} \cdot a$, and $8 \cdot c$, (cf. Table I), so that it would be commensurate with the zero temperature hexon crystal found at $\rho = 0.8895$. The volume and shape of each of the boxes containing the atoms were kept constant for this study. The surface of each box is removed via periodic boundary conditions.[16] The classical equations

of motion were solved for the atoms of unit mass with a fifth-order Gear algorithm.[17] Our time step was never smaller than $\Delta t = 0.002$, and we always conserved the energy for at least eight decimal digits during each run. Since both $u(r)$ and $u_0(r)$ have finite range, we did not require the minimum image or any other cutoff convention.

We began our molecular dynamics studies with a search for $T^{(m)}$, the melting temperature of the hexon crystal. We found $T^{(m)}$ by repeating the following momenta rescaling procedure: Increase the momenta by 2%, advance the trajectory by 450 time steps, and then collect averages for another 500 time steps at that temperature. In this way we produced the plot of the internal energy Φ vs T shown in Fig. 7(a). From the loop[18] in Fig. 7(a) we estimate the melting temperature as $T^{(m)} = 0.53 \pm 0.04$. In the same way, we produced, for the core system, the plot of Φ_0 vs T in Fig. 7(b), from which we estimate the melting temperature of the core solid as $T_0^{(m)} = 0.40 \pm 0.01$.

This procedure for finding the melting temperatures also shows us how stable are both of the crystal structures. By examining both the radial distribution function and the average square displacements, we find that the hexon and core solids retain, respectively, at all temperatures up to their melting points, simple hexagonal and body-centered cubic structures. Further, the pressure was positive for both systems at every positive temperature which we examined.

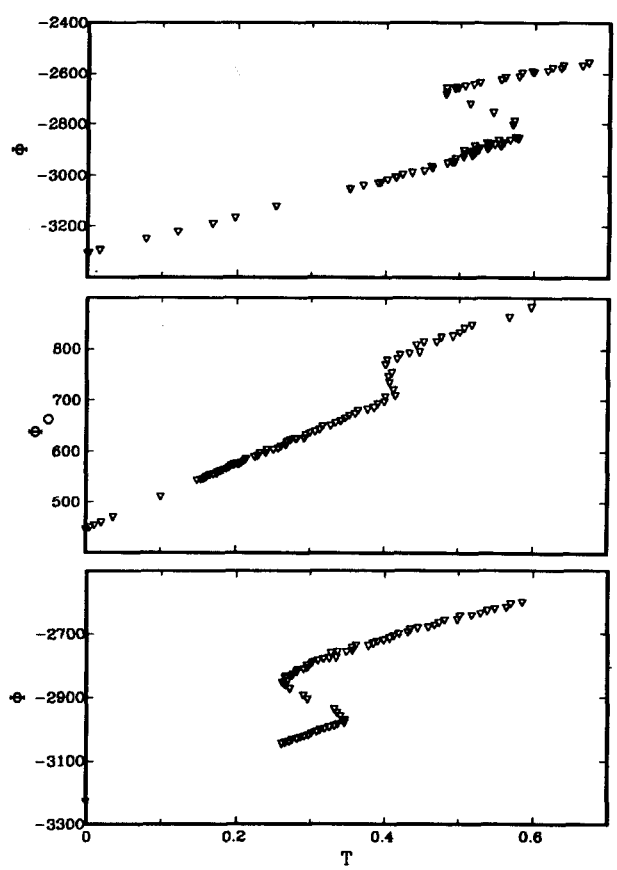

FIG. 7. The average potential energy Φ as a function of temperature for (from top to bottom) (a) the melting of the hexon solid, (b) the melting of the core solid, and (c) the spontaneous freezing of the hexon liquid.

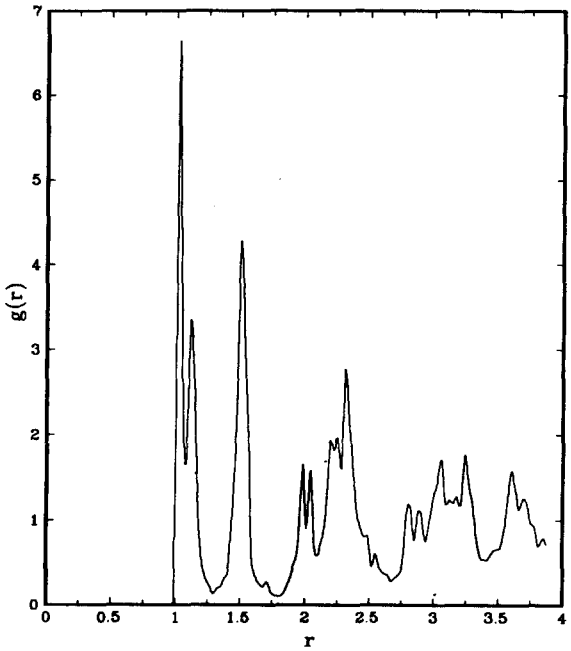

FIG. 8. The radial distribution function for a hexon solid at $T = 5 \times 10^{-8}$ and $\rho = 0.8895$. The solid was produced by quenching a hexon solid at $T = 0.26$. The solid at $T = 0.26$ was the result of the spontaneous freezing of the liquid hexon, as illustrated in Fig. 7(c).

A final confirmation of the simple hexagonal structure for hexon can be found in our attempt to crystallize the liquid hexon. We began with the liquid at $T = 1.13T^{(m)}$ which had been run for 7000 time steps, so that it was well equilibrated. Then we reversed the momenta rescaling procedure used to melt the crystal, except that we collected averages for 1000 rather than 500 time steps. The plot of Φ vs T is shown in Fig. 7(c). The spontaneous transition to a solid occurs near $T = 0.30$. We quenched the solid at $T = 0.26$ by resetting the momenta to zero at random intervals between 50 and 500 time steps. The resulting $g(r)$, which is plotted in Fig. 8, does indeed look very much like the $g(r)$ for the simple hexagonal crystal, but not like those of the other crystals. In fact, as the x–z projection of the simulation box (plotted in Fig. 9) shows, we have produced a simple hexagonal (but rotated) structure with a grain boundary which is nearly coplanar with the x–y plane. On either side of the boundary, the only phase which has nucleated is a strained simple hexagonal solid.

We may now begin our comparison of $g(r)$ and $g_0(r)$ for the hexon solid slightly below $T^{(m)}$ and for the liquid slightly above $T^{(m)}$.

VI. THE VAN DER WAALS PICTURE FOR HEXON NEAR $T^{(m)}$

As we have already observed, neither the hexon nor the core solid undergoes a structural transformation before their respective melting temperatures. Therefore the van der Waals picture is a thoroughly inappropriate description of the hexon solid even near its melting point. We

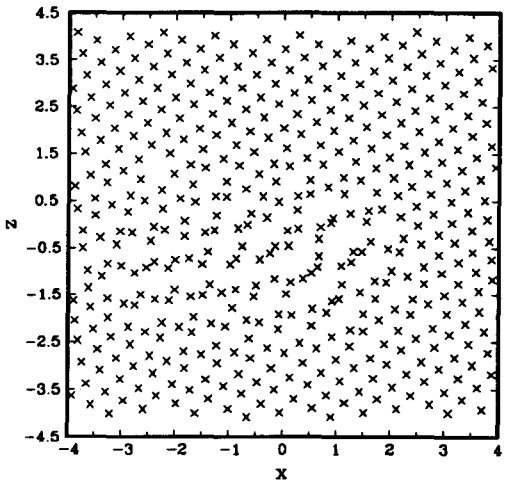

FIG. 9. Projection of the x and z coordinates of the atoms in the quenched hexon solid, whose radial distribution function is illustrated in Fig. 8.

illustrate the differences between the two structures in Fig. 10, where we show both $g(r)$ and $g_0(r)$ at, respectively, $T = 0.35$ and $T = 0.36$. Even so, we might suppose that there may be many liquids which may be accurately described by the van der Waals picture, while the corresponding solids may not be so described. Our goal is, really, to test the van der Waals picture for the liquid.

Our test of the van der Waals picture for liquid hexon is centered on the comparison between $g(r)$ and $g_0(r)$ at a temperature slightly above $T^{(m)}$. We chose $T = 0.60$ for each liquid, which is about 13% above $T^{(m)}$. We calculated $g(r)$ and $g_0(r)$ from runs of 5000 time steps each. We show the resulting radial distribution functions in Fig. 11. For comparison, we show in Fig. 12 the $g(r)$

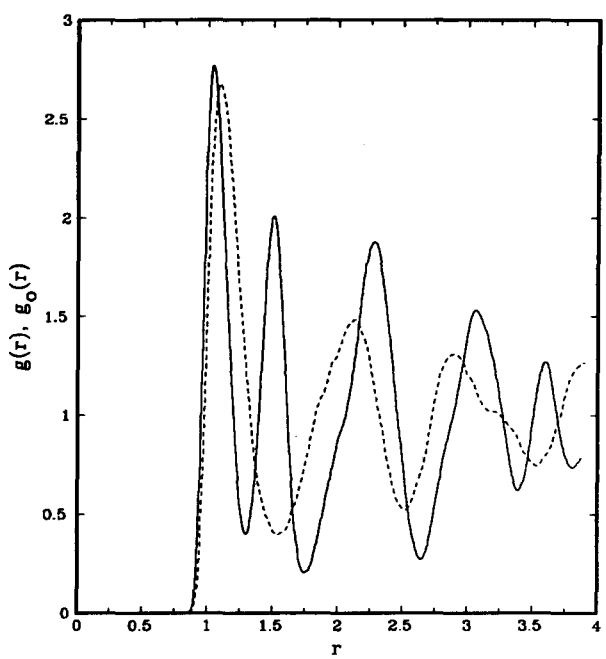

FIG. 10. The radial distribution functions for both the hexon solid (solid curve) and the core solid (dashed curve) at respectively $T = 0.35$ and $T = 0.36$, and $\rho = 0.8895$.

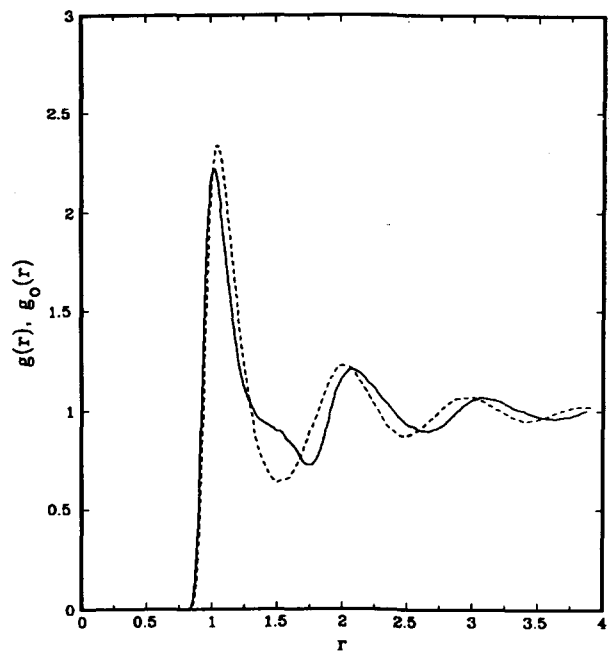

FIG. 11. The radial distribution functions for both the hexon liquid (solid curve) and the core liquid (dashed curve) at $T = 0.60$, and $\rho = 0.8895$.

and $g_0(r)$ calculated by Weeks and Broughton[4] for the Lennard-Jones liquid at $T = 0.75$ and $\rho = 0.87$. In several respects, the $g(r)$ for the hexon liquid is qualitatively different from $g_0(r)$. The peak heights and positions are noticeably different, as are depths and positions of the minima. The first peak of $g(r)$ has a prominent shoulder entirely missing in the first peak of $g_0(r)$. In fact, the shoulder occurs where $g_0(r)$ reaches its first minimum. The first peak of $g(r)$ has also been shifted in such a way as to indicate that the diameter of the hexon atom is effectively smaller than that of the core atom. While the second peak of $g_0(r)$ is symmetrical near its top, the second peak of $g(r)$ is asymmetrical, with a ramp on the

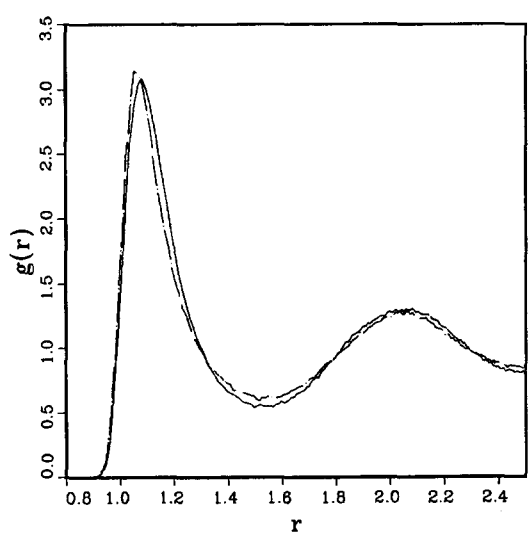

FIG. 12. The radial distribution functions for both the Lennard-Jones liquid (solid curve) and the Lennard-Jones core liquid (chain-dot curve), at $T = 0.75$ and $\rho = 0.87$. Reproduced from Ref. 4 with permission.

right-hand side of the peak. While the first peak of $g(r)$ is closer to the origin than that of $g_0(r)$, the second peak is farther from the origin than that of $g_0(r)$. Even the solid Lennard-Jones system conforms more readily to the van der Waals picture than does the liquid hexon at 13% above its melting temperature, as we can see from Fig. 13. The van der Waals picture plainly cannot do justice to the unusual structure of the hexon liquid near its triple-point temperature. Here we will not exhaustively search for the lowest temperature for which the van der Waals picture is appropriate, although the van der Waals picture certainly becomes accurate for temperatures above $4 \cdot T^{(m)}$. We note, however, that both the shoulder on the first peak and the asymmetry of the second peak still can be seen at temperatures as high as twice $T^{(m)}$.

Although the van der Waals picture gives an inaccurate picture of the structure of the hexon liquid, it can accurately predict values for thermodynamic parameters. For example, the excess (over ideal gas) internal energy per particle ϕ can be calculated from $g(r)$ by the following formula,[9]

$$\phi = (\rho/2) \int d\mathbf{r}\, u(r) g(r).$$

The van der Waals approximation to ϕ is in error by the following term,

$$\Delta\phi = (\rho/2) \int d\mathbf{r}\, u(r)[g(r) - g_0(r)].$$

The error $\Delta\phi$ for the Lennard-Jones liquid is less than 1% of ϕ for densities and temperatures near the triple point.[19] For liquid hexon at $T = 0.60$ and $\rho = 0.8895$, the error is only about 3% of ϕ. The explanation for this begins with a glance at Fig. 14, where we show $[g(r) - g_0(r)]$. The integrand of $\Delta\phi$ varies rapidly, but in such a way that the variations cancel to a great degree when it is integrated. We expect that the errors in the corresponding van der Waals approximation[1,2,4] to the Helmholtz free energy will also be small.

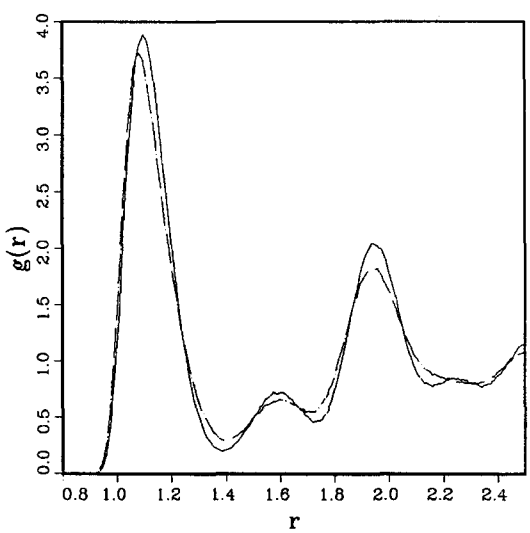

FIG. 13. The radial distribution functions for both the Lennard-Jones solid (solid curve) and the Lennard-Jones core solid (chain-dot curve), at $T = 0.75$ and $\rho = 0.98$. Reproduced from Ref. 4 with permission.

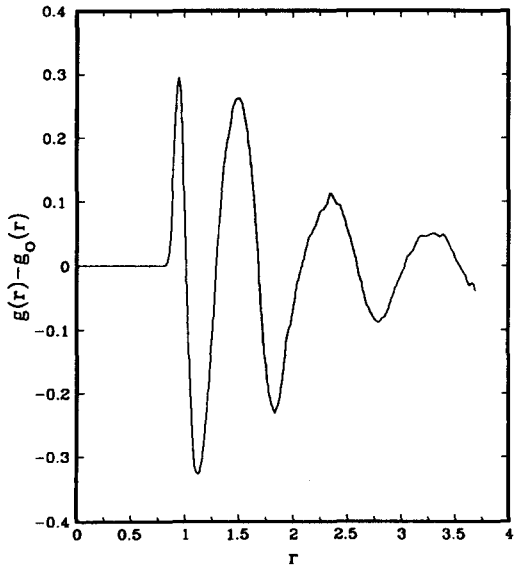

FIG. 14. The difference $g(r) - g_0(r)$, from Fig. 11.

VII. CONCLUSIONS

The attractive force in the hexon model balances the repulsive force in such a way that both the solid and liquid structures are qualitatively different from those anticipated in the van der Waals picture. This disruptive balance can be partly understood in terms of the shape of the hexon potential, which is markedly different from the Lennard-Jones potential in at least one aspect. The "bowl" about the minimum r_e is much wider for the hexon potential than for the Lennard-Jones potential. One measure of this is the force constant $u''(r_e)$, which for hexon is 1/5 the value for the Lennard-Jones model. As a result, the attractive force is strongest much further out [cf. Figs. 1(b) and 2(b)] from the diameter of the hexon atom than it is for the Lennard-Jones model. In the liquid hexon, this distance corresponds to a distance about halfway between the second and third neighbors surrounding the central hexon atom. By contrast, the maximum attractive force for the Lennard-Jones model nearly coincides with the average nearest-neighbor distance in the Lennard-Jones liquid. Now it is easier to see why the attractive force has such a remarkable effect in the hexon liquid while having virtually no impact on the structure of the Lennard-Jones liquid. For both models, the centers of the first peak of $g(r)$ and $g_0(r)$ nearly coincide. Apparently, the attractive forces in both models are so weak that in a dense liquid, essentially only the repulsions set the nearest-neighbor distance. So the attractive force is virtually irrelevant to the structure of a Lennard-Jones solid or liquid, for it operates most strongly at a distance which has already been determined by the repulsive force. Further, beyond that distance, the attractive force so rapidly attenuates that the attractive part of the Lennard-Jones potential becomes nothing more than a uniform background. On the other hand, even a relatively weak attractive force can balance the repulsions in an important way if, as in the case of hexon, it is strongest

well beyond the average nearest-neighbor distance, i.e., well beyond where the repulsive force has its maximum impact.

This explanation of the failure of the van der Waals picture for hexon appears limited to those cases where $g(r)$ for the liquid is already known, for it is from $g(r)$ that we found the average nearest-neighbor distance in the liquid. However, in retrospect, the explanation above really only would have required a knowledge of the structure of the harmonic solid, since the nearest-neighbor distance found in the harmonic solid turns out so close to that found in the liquid. The structure of the harmonic solid can usually be found far more economically than the radial distribution function of the liquid.

One important lesson from this work, then, is that those who study the liquid state can learn more from the solid state than they usually do. The fact that hexon crystallized into such a loosely-packed structure would have been enough indication of the importance of attractive forces, at least for the solid, since repulsive forces alone usually produce much more closely-packed structures. Further, many of those structural features unique to the hexon solid persist in the liquid near its triple point. This too is an indication of how structured the hexon liquid is, and to that extent, how important the attractions are. Finally, in view of our explanation for the success and failure of the van der Waals picture, an understanding of the solid's structure can give an economical zero-order understanding of the balance of the many forces which are involved in the structure of liquids.

We also hope that these results will be encouraging to those who attempt to understand the liquid state in terms of their "inherent structures," as defined by Stillinger and Weber. If even the harmonic crystal can play an important role in our understanding of the hexon liquid, all the more should the inherent structures of liquid hexon be considered important. Although the details fall outside the scope of this paper, we note that our preliminary results indicate that both the hexon model and its core model exhibit temperature-independent inherent structures for their liquids. These structures resemble defective versions of the corresponding crystals. This behavior is the same as has been observed in application of the technique to other atomic substances.[20]

ACKNOWLEDGMENTS

We are grateful to John Weeks for his helpful and challenging comments throughout the course of this work. He also gave us permission to reproduce Figs. 2 and 4 from Ref. 4. We are also grateful to Sidney Abrahams and Philip Marsh for directing our attention to Ref. 13. Finally, we thank Tom Weber for his advice and assistance.

[1] D. Chandler, J. D. Weeks, and H. C. Andersen, Science **220,** 787 (1983).
[2] H. C. Andersen, D. Chandler, and J. D. Weeks, Adv. Chem. Phys. **34,** 105 (1976).
[3] J. L. Lebowitz and E. M. Waisman, Phys. Today **33,** 24 (1980).
[4] J. D. Weeks and J. Q. Broughton, J. Chem. Phys. **78,** 4197 (1983).
[5] D. Chandler, Faraday Discuss. Chem. Soc. **66,** 78 (1978).
[6] F. H. Stillinger and T. A. Weber, Phys. Rev. A **28,** 2408 (1983).
[7] For an example of such a test for the Lennard-Jones model, see L. F. Rull, F. Cuadros, and J. J. Morales, Phys. Rev. A **30,** 2781 (1984).
[8] Reference 1, p. 778.
[9] J.-P. Hansen and I. R. McDonald, *Theory of Simple Liquids* (Academic, London, 1976), Chap. 5.
[10] See Ref. 3 for a discussion of the Kac potential, which conforms exactly to the van der Waals picture.
[11] N. W. Ashcroft and N. D. Mermin, *Solid State Physics* (Saunders College, Philadelphia, 1976), Chap. 4.
[12] R. Fletcher, *Practical Methods of Optimization* (Wiley, New York, 1980).
[13] There are many inorganic compounds at low pressures with crystal structures belonging to the $P6/mmm$ space group, and with c/a ratios near those for hexon. However, none are spherically symmetric compounds. For example, the compound (CuGe)Sm has a simple hexagonal structure, with a c/a ratio of 0.9041. See *Crystal Data,* 3rd ed., edited by H. M. Ondik and A. D. Mighell, Natl. Bur. Stand. (U.S. GPO, Washington D.C., 1978), Vol. 4, p. H/R-91. At high pressures, silicon has been observed to exhibit a simple hexagonal structure with a c/a ratio of 0.94. See J. Z. Hu and I. L. Spain, Solid State Comm. **51,** 263 (1984).
[14] The purely repulsive Gaussian-core model, for certain densities at $T = 0$, produces a bcc lattice. See F. H. Stillinger, Phys. Rev. B **20,** 299 (1979).
[15] The repulsive part of the Lennard-Jones model produces a face-centered cubic crystal, while the crystal structure for the full Lennard-Jones potential is hexagonal close packed, at zero temperature and pressure. See J. O. Hirschfelder, C. F. Curtiss, and R. B. Bird, *Molecular Theory of Gases and Liquids* (Wiley, New York, 1954), p. 1041.
[16] Reference 9, Chap. 3.
[17] C. W. Gear, *Numerical Initial-Value Problems in Ordinary Differential Equations* (Prentice–Hall, Englewood Cliffs, New Jersey, 1971).
[18] The loop becomes a true discontinuity in Φ for decreasing cooling rates.
[19] L. Verlet and J. J. Weiss, Phys. Rev. A **5,** 939 (1972).
[20] F. H. Stillinger and T. A. Weber, J. Chem. Phys. **80,** 4434 (1984).